Genome-wide identification and expression analysis of the LBD gene family in Jasminum sambac

Ji Huang

649252488@qq.com

South China Agricultural University

Qun Su

Guangxi Academy of Agricultural Science

Mingyan Sun

Guangxi Academy of Agricultural Science

Yiqing Zheng

Guangxi Academy of Agricultural Science

Yanhua Zeng

Guangxi Academy of Agricultural Science

Chunniu Li

Guangxi Academy of Agricultural Science

Zide Jiang

South China Agricultural University

Zhaoyang Bu

Guangxi Academy of Agricultural Science

Article

Keywords: LBD gene family; Jasminum sambac; Sclerotium rolfsii; transcriptome; hormone profiling

Posted Date: October 30th, 2025

DOI: https://doi.org/10.21203/rs.3.rs-7770306/v1

Additional Declarations: No competing interests reported.

Version of Record: A version of this preprint was published at Scientific Reports on June 3rd, 2026. See the published version at https://doi.org/10.1038/s41598-026-40654-9.

Genome-wide identification and expression analysis of the LBD gene family in Jasminum sambac

Ji Huang[1,2,+], Qun Su[2,+], Mingyan Sun[2], Yiqing Zheng[2],Yanhua Zeng[2], Chunniu Li[2,*], Zide Jiang[1,*], and Zhaoyang Bu[2,*]

1 South China Agricultural University, College of Plant Protection, Guangzhou 510642, China

2 Guangxi Academy of Agricultural Sciences, Flowers Research Institute, Nanning 530007, China

*corresponding author

email: 649252488@qq.com

+ these authors contributed equally to this work

Abstract

Jasminum sambac (L.) Ait is widely cultivated for its ornamental, medicinal, and economic value. However, infection by *Sclerotium rolfsii* often causes stem and root rot, severely affecting yield and quality. In this study, transcriptome and hormone profiling analyses, combined with a systematic characterization of the LBD gene family, were performed to investigate the molecular responses of *J. sambac* during the early stages of *S. rolfsii* infection. The results showed that four key genes (*DjLBD09*, *DjLBD13*, *DjLBD17*, and *DjLBD28*) exhibited significant differential expression at the early infection stage, and their expression patterns detected by qPCR were highly consistent with RNA-seq data, confirming the reliability of the transcriptome analysis. Integrated metabolomic and transcriptomic analyses further suggested that these LBD genes may participate in regulating signal transduction and defense-related metabolic pathways, thereby playing central roles in early defense responses. This study not only elucidates the molecular mechanisms underlying early defense against *S. rolfsii* in *J. sambac* but also provides potential targets and theoretical support for genetic improvement of disease resistance.

Keywords: LBD gene family; *Jasminum sambac*; *Sclerotium rolfsii*; transcriptome; hormone profiling

Introduction

Jasmine (*Jasminum sambac* (L.) Aiton) is a major ornamental species in the family Oleaceae and genus *Jasminum*. It carries ornamental, medicinal, and economic value: a renowned raw material for scented tea and fragrances, with broad applications in horticulture and wellness, hence the epithet “the first fragrance under heaven”[1]. China has a

long history of jasmine cultivation, with major production areas in Guangxi, Fujian, Sichuan, and Yunnan; among them, Heng County (Guangxi) and Qianwei County (Sichuan) are typical concentrated production regions[2]. However, as the industry has expanded, jasmine production has come under serious threat from diseases, especially southern blight caused by *Sclerotium rolfsii* Sacc.[3].

Southern blight is a destructive, soil-borne fungal disease with a very broad host range, infecting more than 500 plant species, including jasmine, peanut, tomato, and sunflower[3]. In the main jasmine-growing regions of southern China, its incidence has risen year by year and has become a key constraint on yield and quality[7]. The disease typically initiates at the stem base, where white, web-like mycelia develop and brown sclerotia form; it causes basal/root rot and can lead to whole-plant death[2]. Because sclerotia can persist for long periods in soil or crop residues and epidemics readily occur under hot, humid conditions, control is challenging[5]. Field surveys reveal substantial variation in cultivar resistance, offering opportunities for the exploitation of resistant germplasm and resistance breeding[15,16].

At present, no chemical agents provide highly effective and durable control of southern blight[6], and biological control is becoming an important alternative. *Trichoderma harzianum* shows significant efficacy against jasmine southern blight[8], and Trichoderma-based biocontrol formulations not only suppress disease but also improve soil microbial community structure and enhance rhizosphere stability[9]. In parallel, agronomic measures (e.g., crop rotation and soil management) and integrated management strategies have been proposed to curb epidemics[6]. Pathogen-secreted virulence factors—such as oxalic acid and polygalacturonases—also play crucial roles in pathogenesis, deepening our understanding of disease mechanisms[17,18].

Beyond external control, intrinsic plant defenses are critical for resisting infection. Multiple hormone signaling pathways are involved, among which jasmonic acid (JA) and salicylic acid (SA) play central roles in induced resistance. For example, during infection of konjac, JA and SA levels rise markedly alongside increased expression of related genes, highlighting the importance of both pathways[10]. Similar findings in other crops point to a general role for JA/SA signaling in resistance to soil-borne diseases[4].

With advances in genomics and transcriptomics, attention has increasingly focused on transcription factors in plant stress responses. The LBD (Lateral Organ Boundaries Domain) gene family comprises plant-specific transcription factors that harbor a highly conserved LOB domain and specifically recognize the “GCGGCG” motif to regulate downstream gene expression[11]. LBD members participate broadly in the development of lateral organs (lateral roots, branches, leaves, floral organs) and also function in stress responses, secondary growth, regeneration, and metabolic regulation[12,13,19,20]. In *Arabidopsis*, AtLBD16, AtLBD18, and AtLBD29 are key components of auxin-mediated lateral root formation[12,19], whereas AtLBD20 is closely associated with susceptibility to certain fungal pathogens[13]. In citrus, the susceptibility gene CsLOB1 has been validated for bacterial canker; its promoter can be directly activated by pathogen TAL effectors, thereby promoting disease development[14]. LBD genes also directly regulate callus formation[21,22] and modulate hormone signaling through interactions with bZIP transcription factors[23]. Collectively, LBD genes are indispensable for plant growth and development and are intimately linked to biotic stress responses, underscoring their value in research on disease resistance. Based on our systematic analysis of the jasmine LBD family, we hypothesize that certain members act early during southern blight infection by modulating signaling transduction and defense-related metabolic pathways.

In summary, southern blight is now a major constraint on the sustainable development of the jasmine industry. Although conventional agronomic and chemical control measures can mitigate losses to some extent, durable solutions will rely on breeding for resistance and deeper elucidation of the underlying molecular mechanisms. Focusing on the early defense response of jasmine to southern blight, this study integrates transcriptomic and metabolomic analyses with a systematic characterization of the LBD gene family to delineate regulatory patterns and provide a theoretical basis and potential targets for resistance breeding in jasmine.

1 Results and Analysis

1.1 Identification and basic properties

We identified 38, 39, and 36 LBD genes in 'Hutou' (Ht), single-petal (Sj), and double-petal (Dj) jasmine, respectively, by combining genome annotation, chromosomal mapping, and BLAST validation. Protein lengths spanned ~142–452 aa, with theoretical pI values centered around ~6.5 and most members showing an instability index >40, suggesting weakly acidic and largely unstable proteins (full statistics in **Table S1**). Gene names were assigned in chromosomal order within each genome.

Table 1. Summary of physicochemical properties and predicted subcellular localization of LBD family proteins in jasmine

Species	No. of LBD genes	Protein length (aa)	MW (kDa)	Theoretical pI	Instability Index	Aliphatic Index	GRAVY	Predicted localization (counts)
Hutou jasmine (HtLBD)	38	152–316 (mean ≈ 215)	16.9–35.2 (mean ≈ 24.6)	4.68–9.28 (mean ≈ 6.65)	36.3–81.9 (mostly >40, unstable)	58–94	–0.80 to 0.00 (hydrophilic)	Nucleus (28), Chloroplast (3), Extracellular (4), Mitochondrion (1), Other (2)
Single-petal jasmine (SjLBD)	39	152–452 (mean ≈ 226)	16.9–50.9 (mean ≈ 26.7)	4.61–9.23 (mean ≈ 6.51)	36.3–77.0	59–94	–0.80 to –0.01	Nucleus (29), Chloroplast (3), Extracellular (3), Mitochondrion (2), Other (2)
Double-petal jasmine (DjLBD)	36	142–315 (mean ≈ 209)	16.9–35.1 (mean ≈ 25.1)	4.61–9.23 (mean ≈ 6.54)	36.3–72.7	58–89	–0.80 to –0.01	Nucleus (27), Chloroplast (3), Extracellular (3), Mitochondrion (2), Other (1)

Note: MW = molecular weight; GRAVY = grand average of hydropathicity.

1.2 Chromosomal distribution of jasmine LBD genes

LBD loci were unevenly distributed across 12 chromosomes in each genome: Ht peaked on chr1 (6 genes), Sj on chr3 (8), and Dj on chr1 (5), with at least one chromosome in each genome harboring a single locus. Because the spatial patterns do not affect downstream conclusions, detailed karyoplots are relegated to **Figure S1**.

1.3 Phylogenetic analysis of the LBD gene family in jasmine

A maximum-likelihood tree built from jasmine and *Arabidopsis* LBD proteins resolved two major classes (Class I, Class II) and seven subfamilies (Figure 1). Class I dominated (118/156; 75.6%), while subfamilies ranged from 13 (II-a) to 35 (I-c) members. All subfamilies contained representatives from Ht/Sj/Dj and *Arabidopsis*, but lineage representation was uneven, consistent with differential expansion.

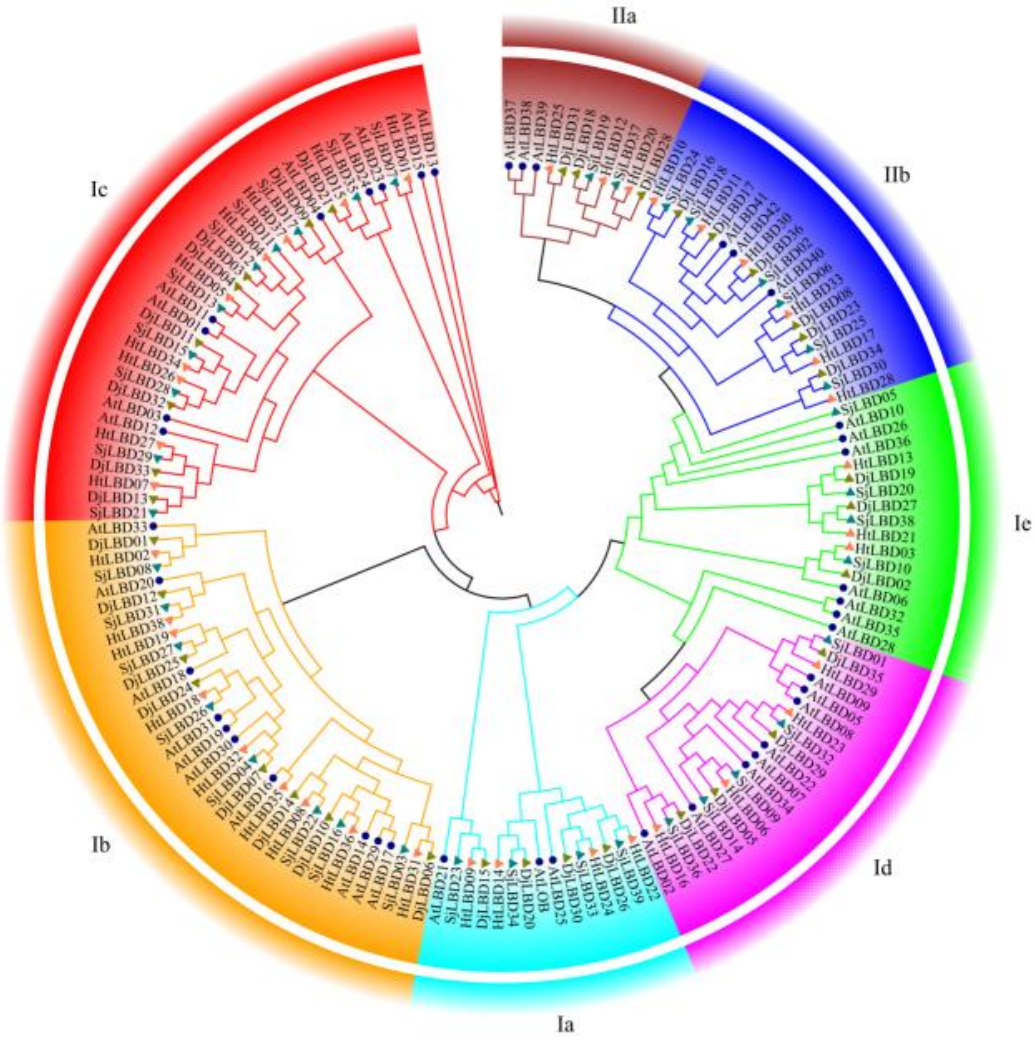

.

Figure 1 Phylogeny of LBD proteins from three jasmine types and *Arabidopsis*

1.4 Gene structure and conserved domain analysis of jasmine LBD genes

Exon–intron architectures were simple (mostly 1–2 exons; a minority with ≥3 in Sj), indicating compact gene models (Figure 2). All proteins harbored the canonical LBD domain; a few carried additional domains (e.g., COG6, PRK11815), hinting at functional diversification. MEME analysis showed motif 1/2 universally present, with diagnostic motifs restricted to specific classes/subfamilies (e.g., Class-II-specific motifs; I-c-specific motifs), and most motifs concentrated toward the C-terminus, suggesting higher C-terminal conservation and N-terminal divergence.

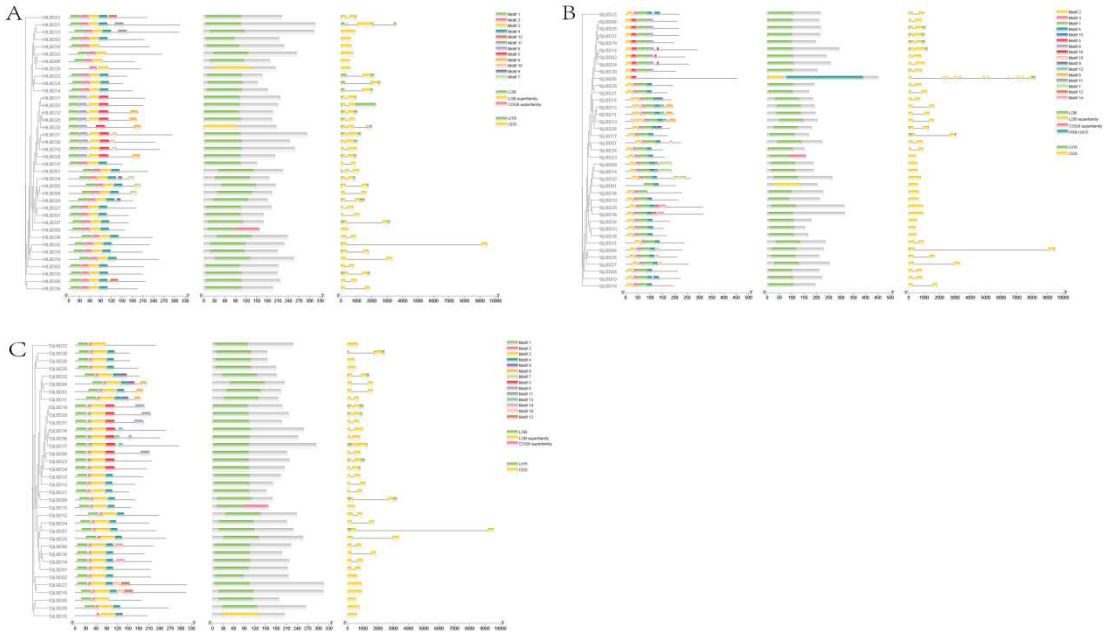

Figure 2 Exon–intron maps, domain architecture, and motif composition of jasmine LBDs.
(A) Hutou jasmine, (B) single-petal jasmine, and (C) double-petal jasmine.

1.5 Cis-acting element analysis in promoters of jasmine LBD genes

Across 2-kb promoters, we detected 22 representative cis-elements related to light, hormone, stress, and development. Light-responsive elements were universal; ~72–77% of genes carried ABA-responsive elements; ~71–72% carried defense/stress motifs; ~50% contained drought-related MYB sites in each genome. Detailed element-by-gene matrices are provided in Figure S2.

1.6 Transcription factor binding site (TFBS) analysis of jasmine LBD promoters

Eighteen TF families were represented in Ht promoters (notably BBR-BPC, Dof, MIKC_MADS with the greatest site counts); Sj and Dj showed largely overlapping TF families, with a few lineage-specific presences (e.g., WRKY unique to Dj). Per-gene TFBS counts varied widely, supporting member-specific regulation. Full heatmaps are provided in Figure S3.

1.7 Collinearity (synteny) analysis of the jasmine LBD gene family

Intra-genome analyses detected 12 duplicated pairs in Ht, 9 in Sj, and 7 in Dj, indicating modest family expansion mainly via segmental/tandem duplication. Inter-genome synteny yielded 55 (Ht–Sj), 52 (Ht–Dj), and 48 (Sj–Dj) orthologous pairs (Figure 3), supporting conserved relationships among cultivars(Full intra-/cross-species panels in Figure S4.). Cross-species macrosynteny with Arabidopsis and rice further corroborated conservation (summary edges shown below; full panels in supplement).

Ka/Ks analysis of syntenic LBD gene pairs revealed that all calculable ratios were <1, indicating purifying selection as the predominant evolutionary force acting on the jasmine LBD family. Specifically, HtLBD pairs showed Ka/Ks values ranging from 0.07–0.23, SjLBD pairs from 0.09–0.29, and DjLBD pairs from 0.15–0.28. These results suggest that the expansion of the LBD family in jasmine is largely driven by strong functional constraints rather than positive selection (Table S2).

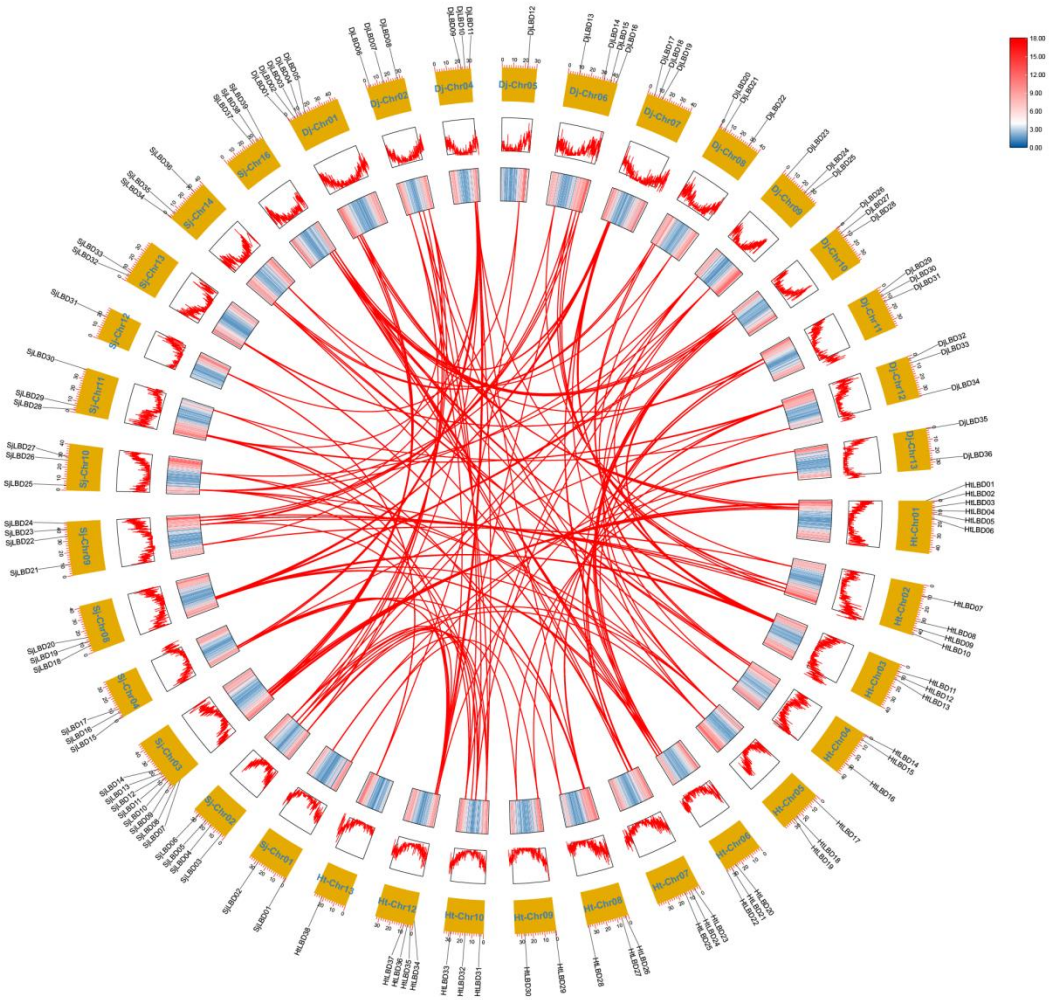

Figure 3 Synteny summary among the three jasmine genomes (single consolidated chord/links panel).

1.8 Endogenous hormone metabolite analysis in jasmine stems after infection with *S. rolfsii*

1.8.1 Principal component analysis

PCA showed that PC1 (48.85%) and PC2 (14.98%) together explained 63.83% of the variance (Figure 4). Samples at 0 h were clearly separated from 48 h and 96 h, while the latter two clustered closely, indicating a strong early metabolic response followed by stabilization.

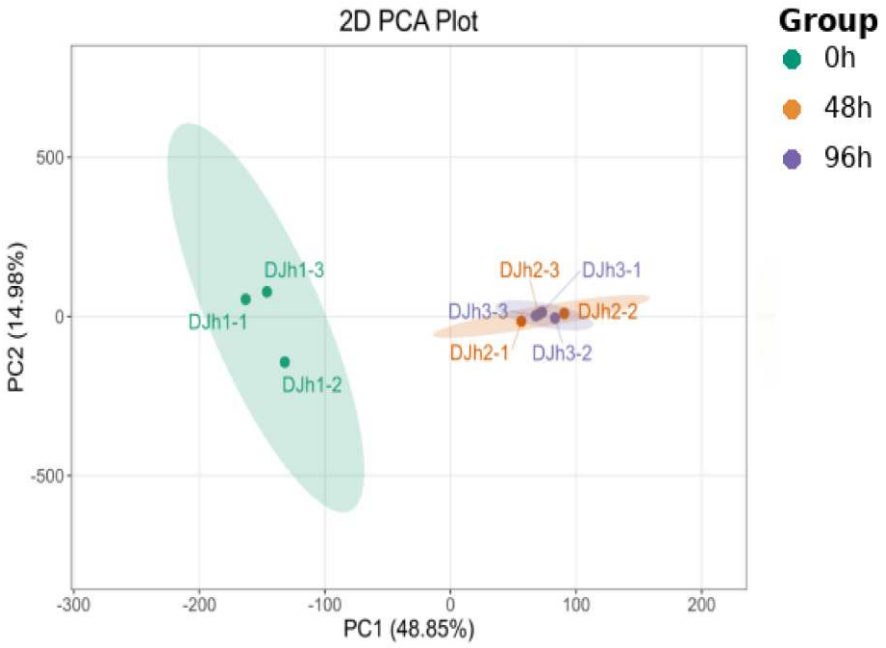

Figure 4. PCA of endogenous hormone metabolites in jasmine stems at different infection stages.

1.8.2 OPLS–DA and permutation validation of metabolomics data from young stems at different stages of infection

OPLS-DA analysis (Figure 5) revealed distinct metabolic profiles among the three time-point comparisons. In A-1/A-2 (0 h vs 48 h), samples were clearly separated, with permutation validation confirming a robust model ($R^2Y = 0.989$, $Q^2 = 0.856$), indicating strong early-stage metabolic reprogramming. In C-1/C-2 (0 h vs 96 h), separation remained evident ($R^2Y = 0.996$, $Q^2 = 0.897$), suggesting sustained alterations. By contrast, in B-1/B-2 (48 h vs 96 h), the difference was weaker ($R^2Y = 0.992$, $Q^2 = 0.802$), implying that after the 48 h peak, the metabolome tended toward stabilization.

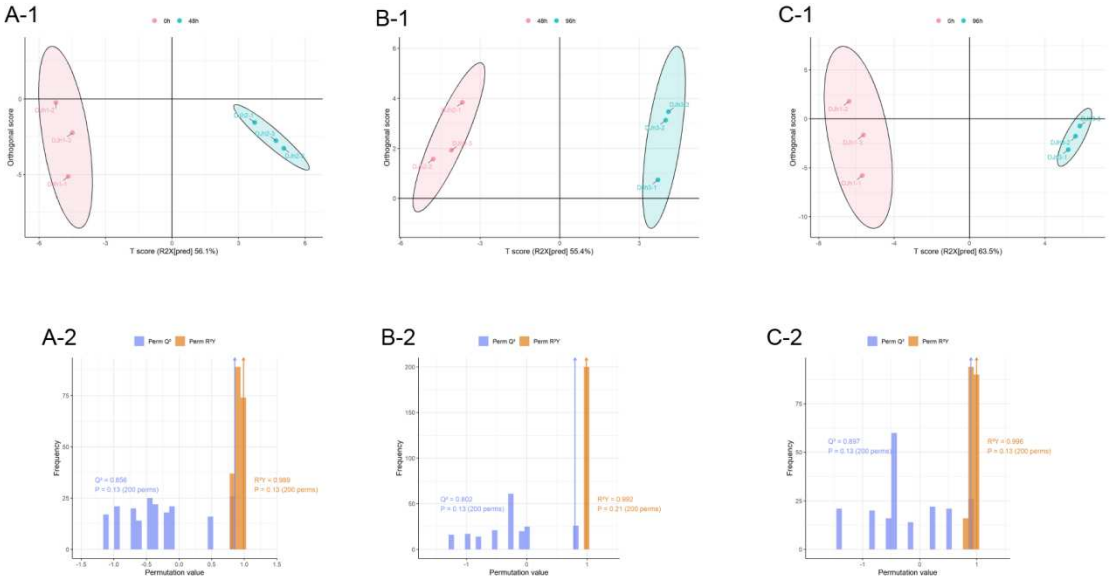

Figure 5. OPLS–DA score plots and permutation tests of hormone metabolites.

1.8.3 Identification of Differential Metabolites

Volcano plots revealed numerous significantly upregulated metabolites in DJh2 (48 h) compared with DJh1 (0 h) (Figure S5). At DJh3 (96 h), upregulation persisted but with reduced intensity. Few differences were observed between DJh2 and DJh3, indicating system stabilization.

Heatmaps further confirmed time-dependent clustering, with strong induction of hormone-related metabolites (JA, OPDA, MEJA, IAA) in DJh2 (48 h), which was partially attenuated in DJh3 (96 h) (Figure 6).

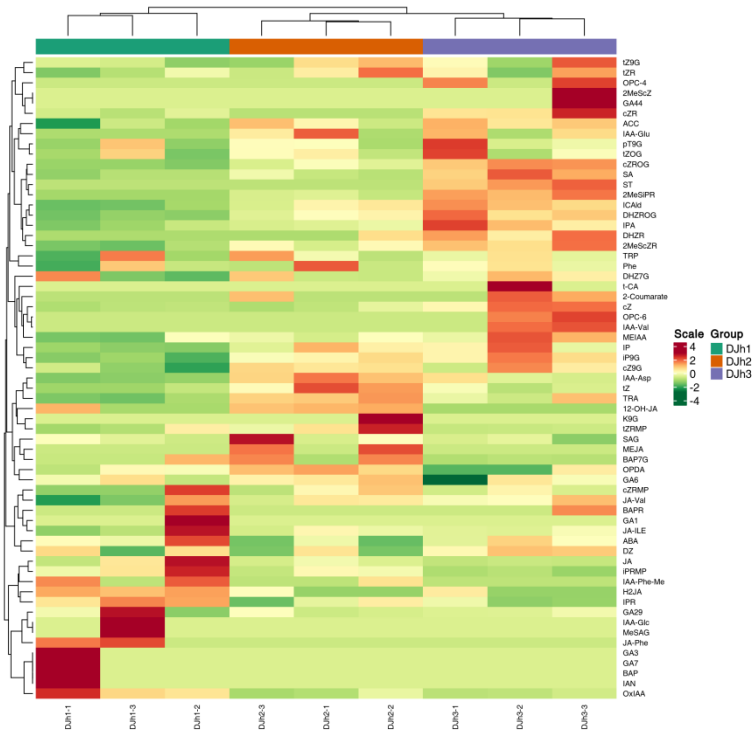

Figure 6. Cluster heatmap of differential metabolites.

1.8.4 KEGG Pathway Enrichment Analysis of Differential Metabolites

Differential metabolites were mainly enriched in fatty acid metabolism, phytohormone signaling, and secondary metabolite biosynthesis. At 48 h, responses centered on α-linolenic acid metabolism and hormone signaling; at 96 h, enrichment extended to phenylpropanoid and carotenoid biosynthesis; by 48–96 h, fewer enriched pathways were detected, consistent with system stabilization (Figure 7).

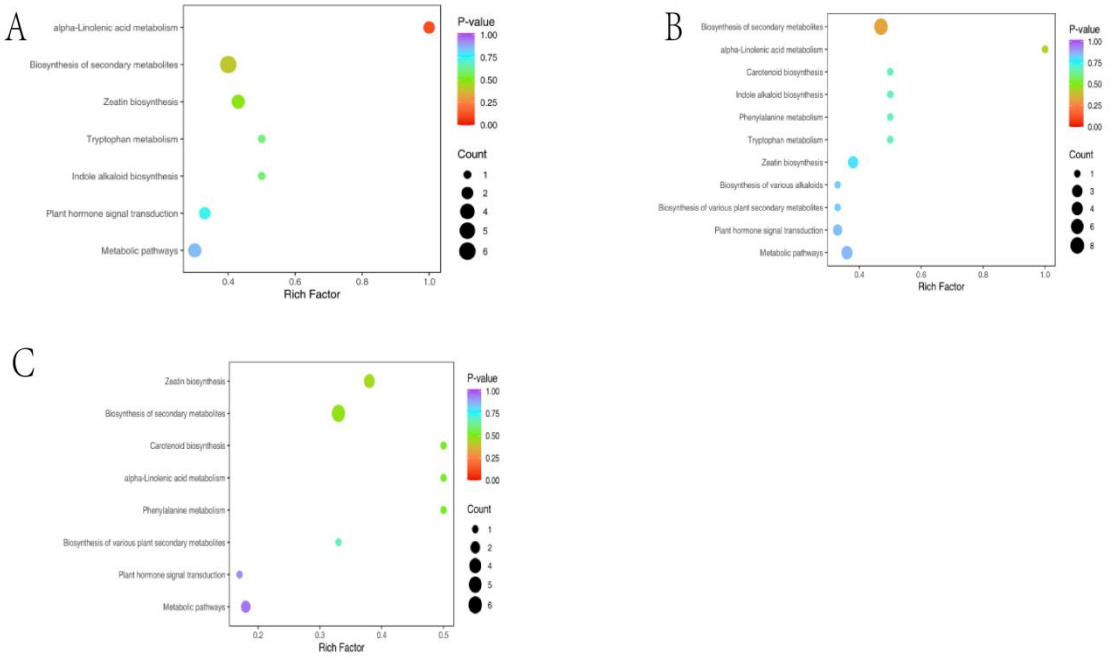

Figure 7. KEGG pathway enrichment of differentially accumulated metabolites (DAMs) in *Jasminum sambac* young stems infected by *Sclerotium rolfsii*.
(A) 0 h vs 48 h, (B) 0 h vs 96 h, and (C) 48 h vs 96 h. Bubble size represents the number of enriched metabolites, and color indicates enrichment significance (P value). Pathway data were obtained from the KEGG database (Kanehisa and Goto, 2000; Kanehisa et al., 2024).

1.9 Transcriptomic Analysis of Jasmine Stems After Infection by *Sclerotium rolfsii*

1.9.1 Differentially Expressed Gene (DEG) Analysis

Across the three pairwise comparisons, transcriptome analysis identified 8,222 DEGs in 0 h vs 48 h (4,546 downregulated, 3,676 upregulated), 8,370 in 0 h vs 96 h (4,654 downregulated, 3,716 upregulated), and only 620 in 48 h vs 96 h (Table 3). These results indicate that the major transcriptional reprogramming occurred within the first 48 h post-infection, characterized by extensive induction and repression of defense- and metabolism-related genes. By contrast, the number of DEGs between 48 h and 96 h was markedly reduced, suggesting that the system gradually stabilized after the early response and transitioned into a phase of regulation and maintenance.

Table 3. Summary statistics of differentially expressed genes

Comparison	Total	Downregulated	Upregulated
0 h vs 48 h	8,222	4,546	3,676
0 h vs 96 h	8,370	4,654	3,716
48 h vs 96 h	620	274	346

1.9.2 GO Enrichment Analysis of Differentially Expressed Genes

GO enrichment showed stage-specific dynamics. In the early stage (DJ1: 0 h vs DJ2: 48 h), DEGs were mainly enriched in photosynthesis-related terms such as “chloroplast thylakoid membrane” and “photosynthesis.” In the mid-stage (DJ1: 0 h vs DJ3: 96 h), these functions were retained but expanded to include “secondary metabolic process” and “transmembrane transporter activity.” In the late stage (DJ2: 48 h vs DJ3: 96 h), fewer DEGs were detected, with enrichment mainly in “cell wall biosynthesis” and “phenylpropanoid metabolism,” reflecting a shift toward structural remodeling. Here, only the overall GO enrichment bubble plot is shown in the main tex(Figure 8), while the three pairwise plots are provided in the supplementary materials(figure S6).

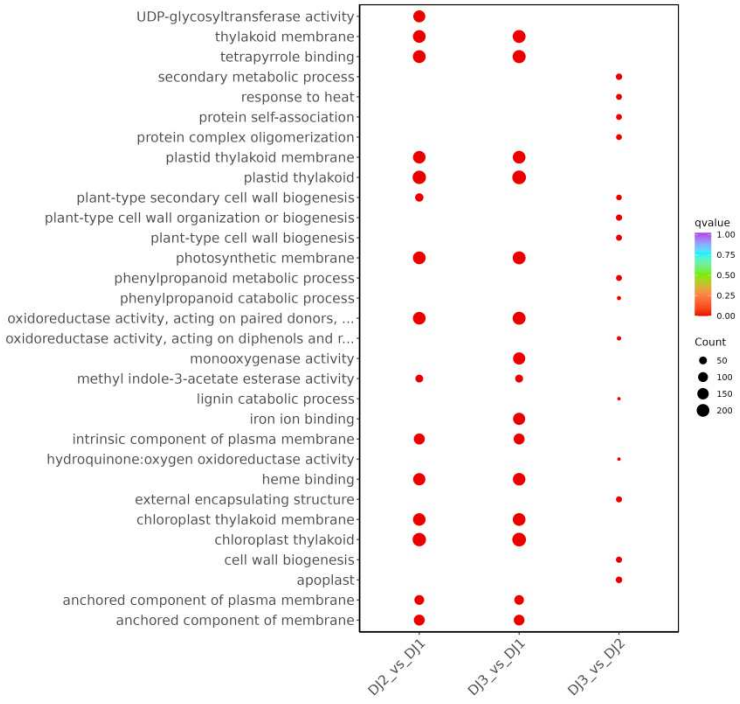

Figure 8. Multi-comparison GO bubble plot of differentially expressed genes.
Note: the x-axis shows the rich factor; bubble size indicates the number of genes; color denotes enrichment significance (Q-value).

1.9.3 KEGG Pathway Enrichment Analysis of Differentially Expressed Genes

KEGG enrichment further highlighted temporal trends. In the early stage (DJ1: 0 h vs DJ2: 48 h), DEGs were enriched in pathways related to secondary metabolism, sugar metabolism, hormone signaling, and photosynthesis. In the mid-stage (DJ1: 0 h vs DJ3: 96 h), enrichment extended to stress-responsive pathways such as glutathione metabolism, while retaining secondary metabolism and hormone signaling. In the late stage (DJ2: 48 h vs DJ3: 96 h), fewer enriched pathways were observed, mainly phenylpropanoid, diterpenoid, and cuticle biosynthesis, reflecting structural remodeling. Notably, secondary metabolism, hormone signaling, and photosynthesis were consistently enriched across all stages, underscoring their central role in defense. Here, only the overall KEGG enrichment bubble plot is shown in the main text(Figure 9), with the three pairwise plots provided in the supplementary materials(Figure S7).

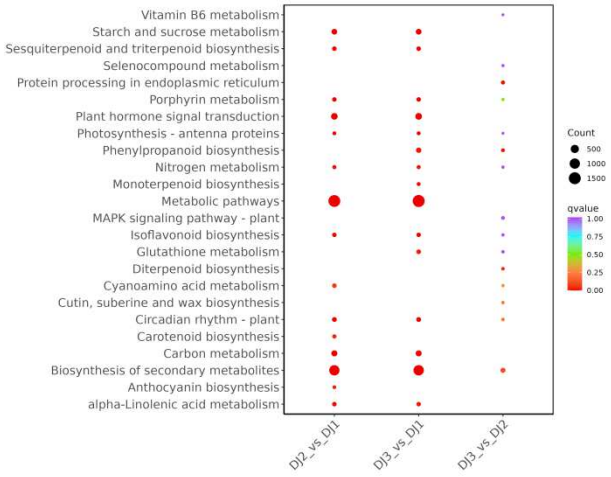

Figure 9. KEGG enrichment of differentially expressed genes (DEGs) from multiple comparisons. Bubble size represents the number of DEGs enriched in each pathway, and color indicates enrichment significance (Q value). Pathway data were obtained from the KEGG database (Kanehisa and Goto, 2000; Kanehisa et al., 2024).

1.9.4 qPCR Validation of Differentially Expressed Genes

qPCR of four LBD genes (DjLBD09, DjLBD13, DjLBD17, DjLBD28) confirmed RNA-seq reliability, with consistent temporal expression patterns: DjLBD09 and DjLBD13 were highly expressed at 0 h, DjLBD17 increased at later stages, and DjLBD28 decreased after infection, suggesting time-specific regulatory roles in defense responses(Figure 10).

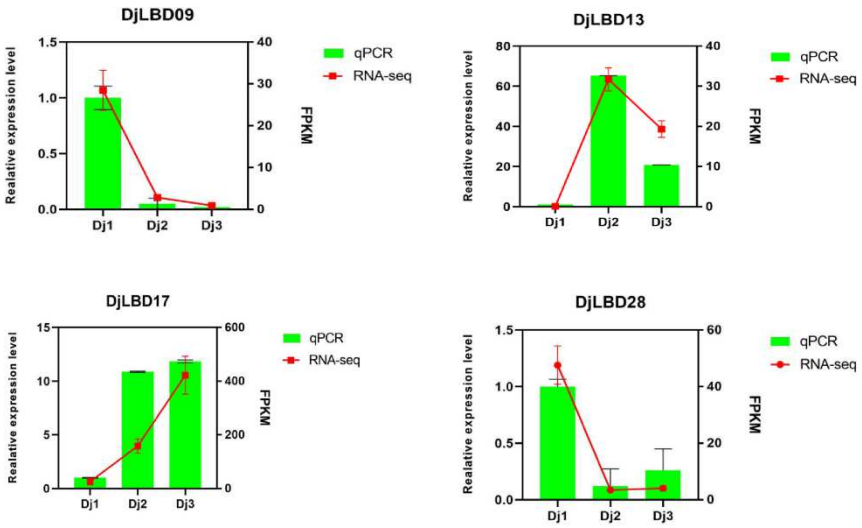

Figure 10. qPCR and RNA-seq validation of four LBD genes (DjLBD09, DjLBD13, DjLBD17, and DjLBD28) in jasmine stems at different infection stages (0 h, 48 h, and 96 h).

1.10 Integrated Metabolomic and Transcriptomic Analysis

1.10.1 KEGG Analysis

Joint KEGG enrichment revealed both shared and time-specific pathways. At 0 h vs 48 h, DEGs and differential metabolites were co-enriched in tryptophan metabolism, zeatin biosynthesis, α-linolenic acid metabolism, plant hormone signaling, and secondary metabolite biosynthesis, reflecting strong early transcription–metabolism

coordination. At 0 h vs 96 h, enrichment patterns remained similar but involved a broader range of pathways, indicating strengthened coordination with prolonged infection. In contrast, 48 h vs 96 h showed markedly fewer shared pathways, mainly restricted to secondary metabolism, α-linolenic acid metabolism, and hormone signaling, suggesting that cross-omics coupling narrows in the late stage (Figure 11).

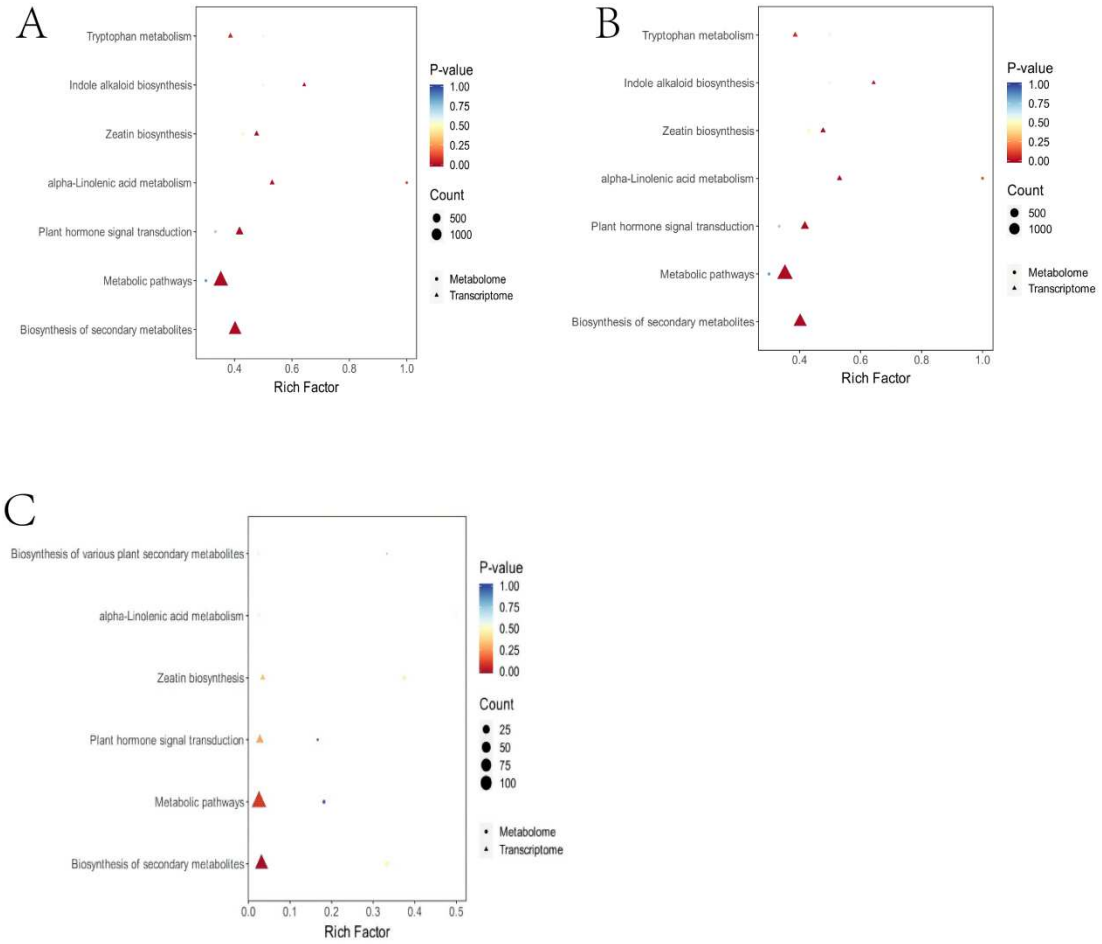

Figure 11. Joint KEGG enrichment of transcriptomic and metabolomic data.
(A) 0 h vs 48 h, (B) 0 h vs 96 h, and (C) 48 h vs 96 h. Circles represent metabolites and triangles represent genes; bubble size indicates the number of differential molecules, and color denotes enrichment significance (P value). Pathway data were obtained from the KEGG database (Kanehisa and Goto, 2000; Kanehisa et al., 2024).

1.10.2 Expression Correlation Analysis

Nine-quadrant plots highlighted strong concordant gene–metabolite changes at 48 h and 96 h compared with 0 h, while 48 h vs 96 h showed reduced significance, consistent with early large-scale reprogramming followed by stabilization. Correlation heatmaps confirmed this trend: early responses were dominated by Auxin, CK, and JA pathways; by 96 h, coupling expanded to include SA signaling; late-stage profiles contracted again, maintaining only a limited set of hormone pathways (Fig. 12–13).

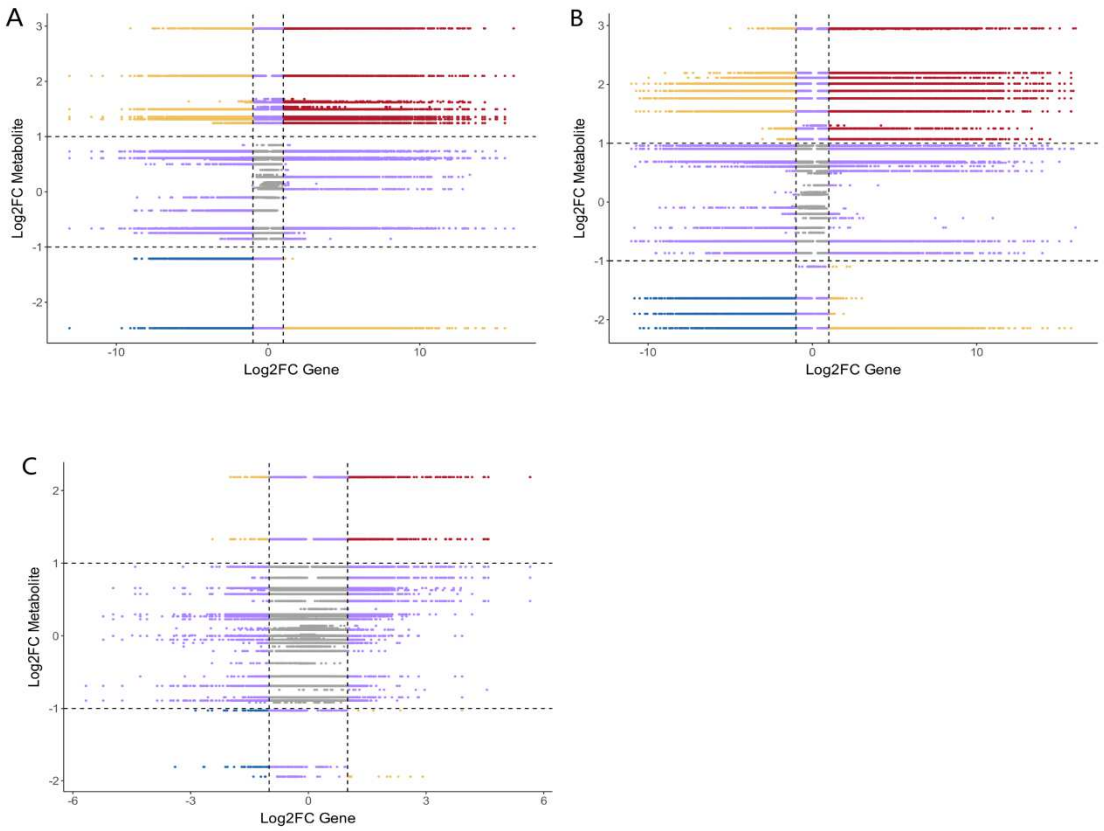

Figure 12. Nine-quadrant plots from the integrated transcriptome–metabolome analysis.
(A) 0 h vs 48 h, (B) 0 h vs 96 h, and (C) 48 h vs 96 h. The x-axis represents gene log2(FC) and the y-axis represents metabolite log2(FC). Points in the upper-right and lower-left quadrants indicate concordant up- or down-regulation, while points in the upper-left and lower-right quadrants indicate opposite changes.

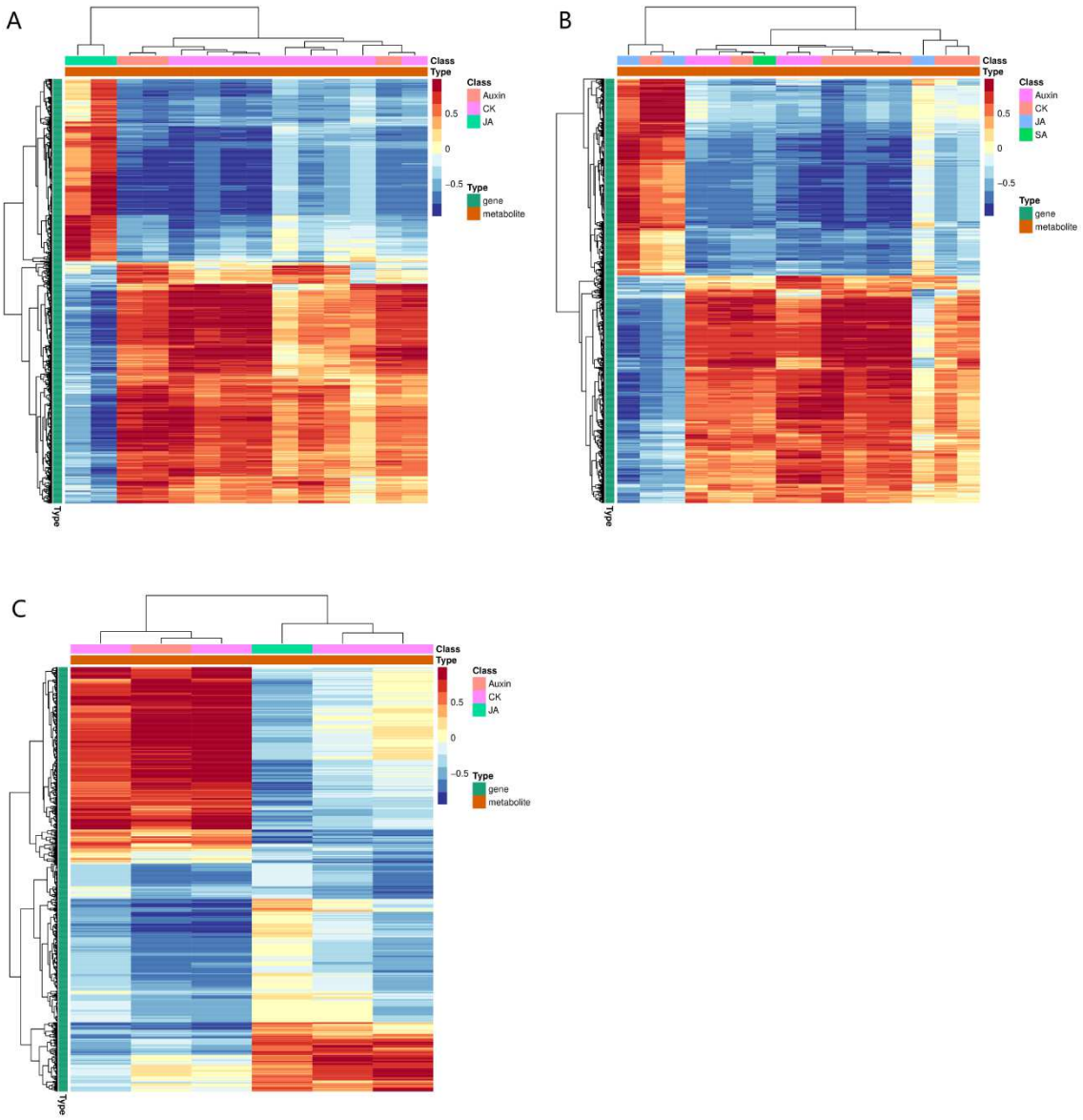

Figure 13. Correlation clustering heatmaps from the integrated transcriptome–metabolome analysis of jasmine stems following *Sclerotium rolfsii* infection.(A) 0 h vs 48 h, (B) 0 h vs 96 h, and (C) 48 h vs 96 h.Colors from blue to red indicate low to high relative expression/abundance levels of genes and metabolites.

(3) CCA Analysis

O2PLS modeling further supported tight transcriptome–metabolome coupling, with high explanatory power (R^2X = 0.9527, R^2Y = 0.9584) and correlation (R^2Xcorr = 0.8836, R^2Ycorr = 0.9281). Hormone-related metabolites (OPDA, MEJA, IAA-Asp) and several DEGs with high loadings contributed strongly, underscoring coordinated regulation of hormone signaling and defense responses (Table 4, Fig. 14).

Table 4. O2PLS model contribution statistics

R2X	R2Y	R2Xcorr	R2Ycorr
0.9527	0.9584	0.8836	0.9281

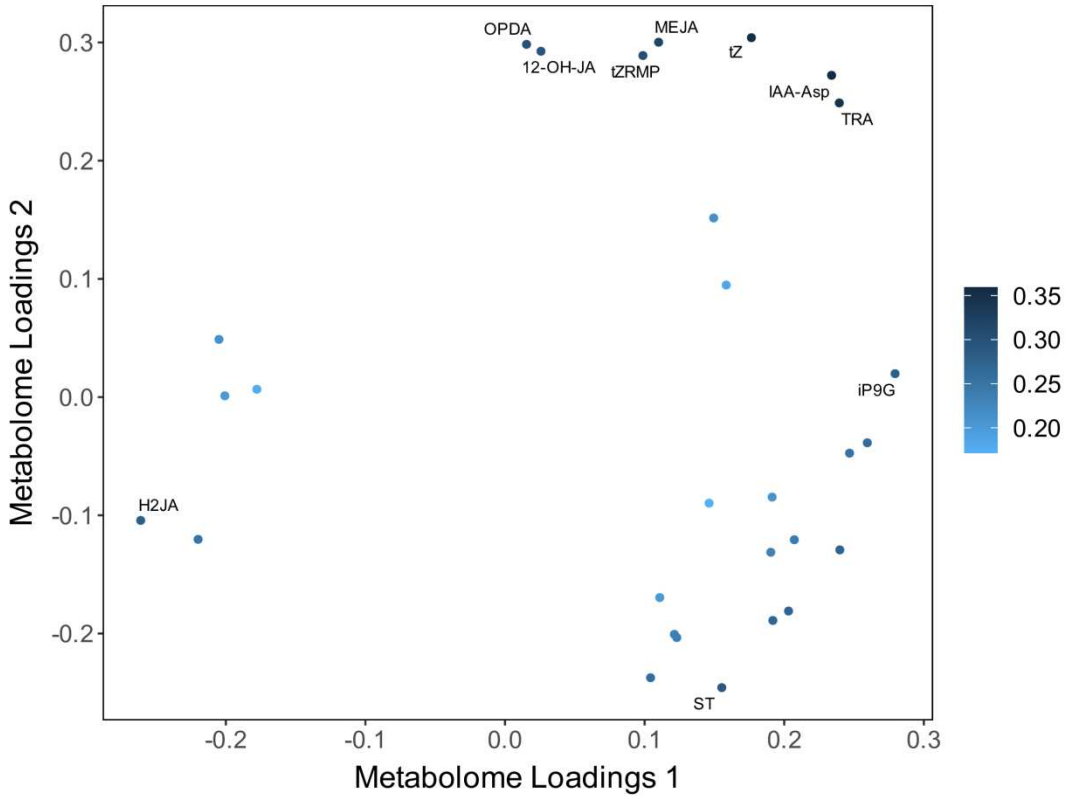

Figure 14-1. Metabolite loadings plot.
Note: color intensity indicates contribution magnitude.

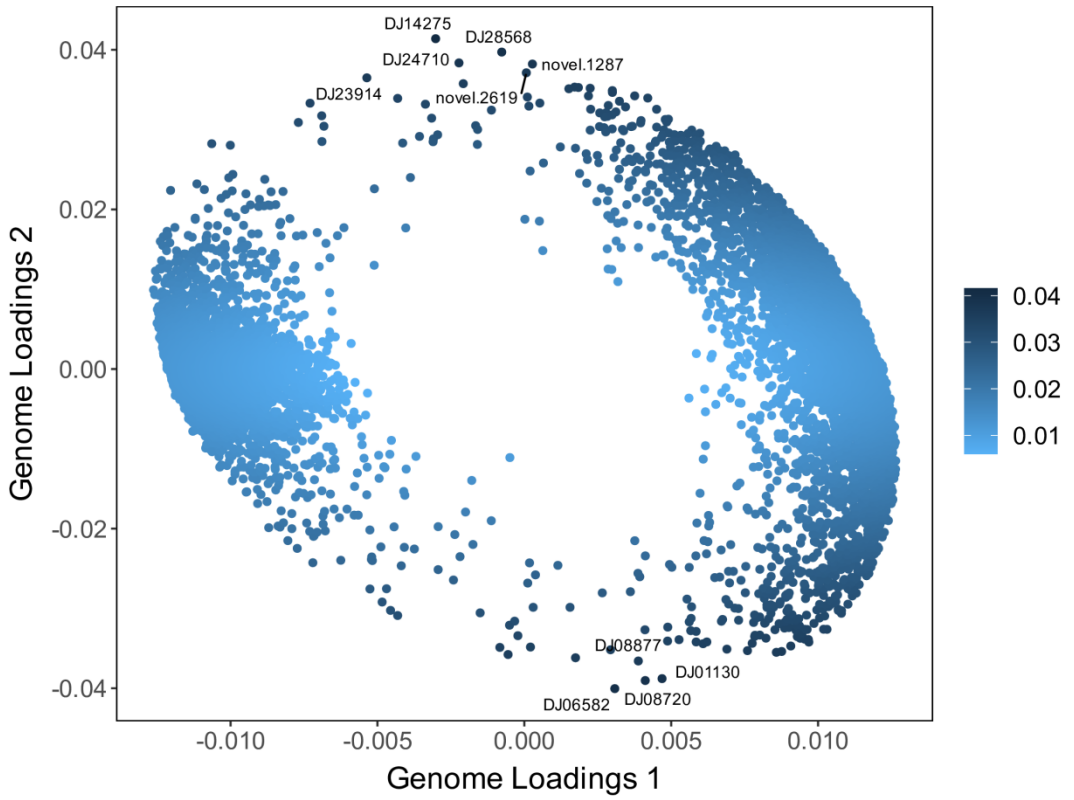

Figure 14-2. Gene loadings plot.
Note: color intensity indicates contribution magnitude.

2 Discussion

This study integrates gene-family characterization, metabolomics, transcriptomics, and cross-omics analyses to delineate the molecular regulatory landscape of jasmine (young stems) under infection by *Sclerotium rolfsii*. We show that the LBD gene family exhibits evolutionary and structural diversity, while both the transcriptome and metabolome undergo pronounced temporal dynamics. The integrated analysis further uncovers putative links between genes and metabolites. Together, these results deepen our understanding of jasmine's disease-resistance biology and underscore the value of multi-omics integration for decoding complex regulatory networks.

Time-series analyses indicate that 48 h post-inoculation represents a peak in transcriptional responses, involving thousands of differentially expressed genes (DEGs) and pointing to a critical early window for signal perception and initiation of defense. By 96 h, the number of DEGs remains large but shows relatively modest changes compared with 48 h, suggesting a trend toward transcriptional steady state. Metabolomics reveals that differential metabolites are mainly enriched in pathways related to energy, amino-acid, and secondary metabolism. The accumulation of multiple hormone- and defense-related metabolites (e.g., jasmonates, ferulic acid, and flavonoids) is consistent with previous studies, supporting tight coupling between early metabolic reprogramming and transcriptional activation, followed by more adaptive regulation at later stages.

The integrated analysis highlights extensive co-variation between genes and metabolites, with highly concordant expression–metabolite patterns in phenylpropanoid metabolism, plant hormone signal transduction, and α-linolenic acid metabolism. Correlation clustering and network results suggest that the transcription factors DjLBD13, DjLBD17, DjLBD28, and DjLBD09 form core regulatory modules with defense-related metabolites, implying that these LBD genes may act upstream to coordinate dynamic changes in downstream pathway genes and metabolites. Notably, although these four LBD genes did not themselves emerge as enriched GO/KEGG terms,

their differential expression was validated by qPCR, lending further support to their roles in pathogen response. O2PLS/CCA modeling also indicates strong correlations between hormone-related metabolites and diverse DEGs, suggesting that the above LBDs may orchestrate defense by modulating hormone and secondary-metabolism pathways.

Based on these results, we propose a dynamic regulatory framework: in the early phase (0–48 h), activation of signaling and defense genes—including LBD transcription factors—drives metabolite biosynthesis and defense responses; in the mid-to-late phase (48–96 h), the system progressively stabilizes, with a smaller subset of genes and metabolites remaining active to sustain adaptation. While this work provides new insights into jasmine's molecular responses to *S. rolfsii*, further functional validation and expanded multi-omics studies are needed to refine the model. Overall, we not only chart the temporal coupling of transcription and metabolism but also propose plausible regulatory mechanisms that will inform future mechanistic studies and metabolic improvement.

3 Conclusions

Through gene-family analysis, metabolomics, transcriptomics, and their integration, this study systematically elucidates the molecular response patterns of jasmine young stems under *S. rolfsii* infection. The interval from 0–48 h constitutes the most drastic stage of transcriptional and metabolic change, involving large numbers of DEGs and differential metabolites and indicating a critical early regulatory window; differences diminish markedly from 48–96 h, suggesting progression toward a steady state. The integrated analysis further reveals strong gene–metabolite concordance in phenylpropanoid metabolism, plant hormone signaling, and α-linolenic acid metabolism, and identifies several key gene–metabolite pairs. In particular, qPCR-validated DjLBD13, DjLBD17, DjLBD28, and DjLBD09 likely play important cross-omics regulatory roles by modulating hormone and defense-related metabolic pathways. This work enriches our understanding of jasmine's molecular mechanisms under *S. rolfsii* infection and provides a valuable reference for subsequent functional validation and metabolic engineering.

4 Materials and Methods

4.1 Materials

4.1.1 Experimental site

Field trials were conducted in the open nursery of the Flower Research Institute, Guangxi Academy of Agricultural Sciences (22°48′ N, 108°22′ E), where new black weed-control fabric had been laid on the ground surface. The site is located in a southern subtropical monsoon climate zone, with a mean annual temperature of 21.6 °C, mean annual precipitation of 1,304.2 mm, mean relative humidity of 79%, and a frost-free period of 334 days[2].

4.1.2 Experimental materials

Three-year-old potted plants of the main local cultivar—Hengxian double-petal jasmine—were used. The jasmine southern blight pathogen (*Sclerotium rolfsii* Sacc.) isolate SRNN1 was obtained from diseased plants collected in Jiaoyi Town, Heng County, Guangxi; after purification and identification, its rDNA-ITS sequence was deposited in GenBank under accession number MT634388. The pathogen was cultured on potato dextrose agar (PDA) composed of: potato 200 g, glucose 20 g, agar 15 g, distilled water 1 L; pH unadjusted ("natural").

4.2 Inoculation with *S. rolfsii* by the stem-adhesion method

Materials included PDA plates fully covered with mycelia, sterile cotton, sterile water (ultrapure; stored in Erlenmeyer flasks and spray bottles), sealing tape, sterile toothpicks, sterile pipette tips, large plastic bags, and jasmine plants.

All procedures were performed with gloves. First, using a sterile pipette tip (large end downward), perforate the PDA from the colony margin and continue until the plate surface is covered; seal the plate and reserve for use within 1 day. Prepare strips of sterile cotton and moisten them with sterile water. With a sterile toothpick, gently score around the intended inoculation site on the stem; remove excess leaves so the wound is exposed without penetrating deeply into the stem. For inoculation, use a new sterile toothpick to pick up an agar plug bearing mycelia and place it onto the moistened cotton with the mycelial surface facing the scored stem. Affix the cotton to the wound, wrap firmly, and secure with sealing tape, keeping the openings at the upper and lower ends as small as possible.

In non-air-conditioned rooms or outside an incubator, a high-humidity microenvironment can be created with a large plastic bag: mist the inner surface, then cover the entire plant with the bag inverted so that water droplets coat the interior. Six hours after inoculation, assess moisture loss, randomly inspect several plants, and add water as needed to determine subsequent watering intervals. To replenish moisture, spray an appropriate amount of sterile water through the upper and lower openings at the tape. After approximately 1–3 days, once stem infection is evident, proceed to the next stage.

4.3 RNA extraction from infected stems

Healthy, uniformly growing jasmine plants were selected. Stems inoculated with *S. rolfsii* served as the treatment group, and samples collected before inoculation (time 0; Day 0) served as the control. Sampling time points were set at pre-inoculation (0 h) and 48 h (Day 2) and 96 h (Day 4) post-inoculation. Three biological replicates were collected per time point, with three stems pooled per replicate. For each sample, 7–8 cm stem segments were cut using sterile pruning shears and divided into two portions: one for RNA extraction and transcriptome analysis, and the other for hormone profiling. Samples were snap-frozen in liquid nitrogen immediately after processing and stored at −80 °C until further use.

4.4 Sequence mining

Genome assemblies of single-petal jasmine, double-petal jasmine, and ‘Hutou’ jasmine were obtained from collaborative institutions. Coding sequences (CDS) and protein sequences were extracted using TBtools[26], and reciprocal searches were performed against the Swiss-Prot database to obtain candidate proteins. In addition, the *Arabidopsis thaliana* genome was downloaded from NCBI (https://www.ncbi.nlm.nih.gov/), and LBD gene sequences were identified based on annotation information.

4.5 Identification of jasmine LBD family members and analysis of physicochemical properties

In total, 39 LBD genes were identified in single-petal jasmine, 36 in double-petal jasmine, and 38 in ‘Hutou’ jasmine. Physicochemical properties of LBD proteins from the three jasmine types were analyzed using Python (Biopython package), and subcellular localization was predicted with Plant-mPLoc (http://www.csbio.sjtu.edu.cn/bioinf/plant-multi/).

4.6 Gene structure, conserved motifs, and domain prediction for the jasmine LBD family

Based on gene annotations, LBD protein sequences from the three jasmine types were obtained. Conserved motifs were predicted using the “Simple MEME Wrapper” in TBtools with default parameters. Gene structure information and motif prediction results were organized and visualized in TBtools.

4.7 Chromosomal localization, phylogenetic tree construction, and sequence alignment

Chromosomal locations of LBD genes were mapped and visualized with TBtools (v2.149) for all three jasmine types. Multiple sequence alignments of LBD proteins were generated using the “One Step Build a ML Tree” function in TBtools, and a phylogenetic tree was constructed based on amino-acid sequence similarity. The tree was visually refined using the Chiplot web tool (https://www.chiplot.online/).

4.8 Cis-acting element prediction in promoters of jasmine LBD genes

Promoter regions (2,000 bp upstream of the transcription start site) of LBD genes from the three jasmine types were retrieved and analyzed for cis-acting regulatory elements using PlantCARE (http://bioinformatics.psb.ugent.be/webtools/plantcare/html)[27]. Predicted elements were categorized and visualized in TBtools.

4.9 Real-time quantitative PCR (qRT–PCR) of jasmine LBD genes

Total RNA extraction and reverse transcription were outsourced to a biotechnology company. The reference gene was **UPL7**[28]. All primers were designed with Primer Premier 6; sequences are listed in **Table 1**.

qRT–PCR was performed on an ABI StepOne Plus instrument in a 20.0 μL reaction containing 0.8 μL each of forward and reverse primers, 10.0 μL of 2× qPCR SYBR Green Master Mix, 1.0 μL cDNA template, and nuclease-free water to 20.0 μL. Cycling conditions were: 95 °C for 30 s; then 40 cycles of 95 °C for 5 s and 60 °C for 10 s. Each sample was run with three technical replicates. Relative transcript levels were calculated using the 2^−ΔΔCt method. Calculations were performed in Excel, and statistical visualization was conducted in GraphPad Prism 8.0.2.The reference gene is UPL7[28]. For label consistency with DjLBD identifiers, we format it as ‘UPL07’ in primer IDs; this is an alias of UPL7.

Table 1. Primer sequences for target and reference genes used in qRT–PCR

Gene	Primer sequences (5′ →3′ ; forward / reverse)
DjLBD09	F: GCACAAGCCGAAGTGGTACA / R: TGACTGGACGATGGGAAGGC
DjLBD13	F: GCAGGAGCTTCCGTTACACC / R: AGCACCAACACAGCCGTAGA
DjLBD17	F: GCCGAGCCATGAGTCGTCTT / R: AGTCTGCCCAGAAACCAAGC
DjLBD28	F: TGCCGAGTTCTCCGAAAGGG / R: ACGGTGGCGTTGCTTTGAG
UPL07 (reference)	F: CAGAAGAGGCTGGTAGATGTCG / R: GCCCTTTCATTCAACAGCAA

Note: ‘UPL07’ is a zero-padded label used for layout consistency and refers to the same gene as UPL7.

4.10 OPLS-DA analysis and model validation

To distinguish metabolic profiles among treatments, orthogonal partial least-squares discriminant analysis (OPLS-DA) was applied to the metabolomics data. Prior to modeling, the data matrix was log-transformed and mean-centered to reduce noise and enhance robustness. Modeling and visualization were performed in R (v4.3.0) using the **ropls** package. Model fit and predictive ability were evaluated by **R^2Y** and **Q^2**, respectively, and reliability was assessed by **200-time permutation testing** to prevent overfitting. When the original model’s R^2Y and Q^2 values exceeded those of the permuted models and the regression line intercept was < 0, the model was considered robust with good predictive performance.

4.11 Transcriptome sequencing and data analysis

RNA-seq and initial data processing were performed by **Wuhan MetWare Biotechnology Co., Ltd.** After total RNA extraction and QC, libraries were sequenced on the Illumina platform. Clean reads were mapped to the reference genome (*Jasminum sambac*, GWHBFHJ00000000)[29,30]. Gene expression levels were quantified as FPKM, and read counting was conducted with **featureCounts**[31]. Differential expression analysis used **DESeq2** with thresholds of $|\log_2FC| \geq 1$ and FDR < 0.05[32]. Results (DEG summaries, volcano plots, GO enrichment, and KEGG pathway enrichment) were used for downstream biological interpretation[33,34].

4.12 Metabolomic analysis

Targeted plant-hormone metabolomics was conducted by **Wuhan MetWare Biotechnology Co., Ltd.** using an LC–MS/MS platform (UPLC: ExionLC™ AD; MS/MS: QTRAP® 6500+). After grinding samples in liquid nitrogen, metabolites were extracted with a methanol/water/formic acid mixture, with internal-standard–based QC following established protocols for plant hormone extraction and preprocessing[35,36,41].

Chromatographic separation employed a C18 column; mobile phases were ultrapure water with 0.04% acetic acid and acetonitrile, with a gradient program adapted from published HPLC/UPLC–MS methods[37,38,40]. Mass spectrometry used an ESI source in both positive and negative modes, with parameters following typical UHPLC–MS/MS hormone assays[40].

Compound identification was based on an in-house library and authentic standards; quantification used **MRM** with external-standard calibration, following protocols for multi-hormone targeted profiling[39,42]. Differential metabolites were selected using combined criteria of **OPLS-DA VIP > 1**, **fold change ≥ 2 or ≤ 0.5**, and **t-test p < 0.05**. Identified differential metabolites were annotated and enriched against **KEGG** to infer pathway-level changes.

4.13 Integrated analysis of metabolome and transcriptome

Integrated analyses were performed by **Wuhan MetWare Biotechnology Co., Ltd.** First, principal component analysis (PCA) of metabolomic and transcriptomic datasets was conducted with the **prcomp** function in R (v4.2.0) to assess global separation among treatments[43]. KEGG annotation and enrichment of DEGs and differential metabolites followed the same tools and settings as in the transcriptome analysis to ensure cross-omics comparability [44].

Pairwise **Pearson correlations** were computed (R **stats** package) to identify significant gene–metabolite

associations with $|r| \geq 0.8$ and $p < 0.05$, visualized using **nine-quadrant plots**, clustered heatmaps (**pheatmap**), and correlation networks (**Cytoscape v3.9.1**) to reveal putative regulatory relationships[45].

At the global level, **canonical correlation analysis (CCA)** (R **CCA** package) was used to characterize canonical variate pairs between the two omes[43]. In parallel, **O2PLS** (R **OmicsPLS** package) decomposed each dataset into joint, orthogonal, and noise components; key drivers were identified based on $\mathbf{R^2}$ and variable **loadings**[46].

References

1. Liu, Q.-Y.; Yang, Z.-W.; Yang, Z.-G.; et al. Occurrence characteristics and control measures of jasmine southern blight. Science Popularization for Rural Development (2018). [in Chinese]

2. Li, C.-N.; Li, X.-M.; Du, C.-J.; et al. Outdoor inoculation technique and potted resistance identification of jasmine southern blight. Chinese Journal of Tropical Crops 42(8): 2350–2355 (2021). [in Chinese]

3. Li, M.; He, L.-M.; Zhao, T.; et al. Research progress on Sclerotium rolfsii. Plant Protection (2020). [in Chinese]

4. Fan, P.-M. Resistance evaluation of peanut to southern blight and transcriptomic/metabolomic analyses. PhD thesis, Chinese Academy of Agricultural Sciences (2021). [in Chinese]

5. Yan, L.-Y.; Song, W.-D.; Zhang, F.; et al. Establishment of greenhouse inoculation techniques for peanut southern blight and identification of seedling resistance. Chinese Journal of Oil Crop Sciences 39(5): 687–692 (2017). [in Chinese]

6. Yang, W.-Y. Preventive measures and treatment methods for jasmine southern blight. Southern Agriculture 15(32): 51–52, 55 (2021). [in Chinese]

7. Chen, K.-R.; Ren, L.; Xu, L.; et al. Research progress on peanut southern blight. Chinese Journal of Oil Crop Sciences 40(2): 302–308 (2018). [in Chinese]

8. Li, L.; Shen, G.-J.; Shao, Z.-H. Biological control of southern blight with Trichoderma harzianum. Journal of Zhejiang Agricultural University 9(3): 221–225 (1983). [in Chinese]

9. Du, C.-J.; Yan, W.-H.; Pan, L.-F.; et al. Effects of Trichoderma-based preparations on southern blight and soil microbial abundance. Bulletin of Chinese Agricultural Science 30(1): 169–173 (2014). [in Chinese]

10. Gao, P.-H.; Qi, Y.; Yang, M.; et al. Effects of southern blight infection on endogenous hormone contents and related gene expression in konjac. Acta Agriculturae Boreali-Sinica 40(3): 149–156 (2025). [in Chinese]

11. Husbands, A.; Bell, E.; Shuai, B.; et al. Lateral organ boundaries defines a new family of DNA-binding transcription factors and can interact with specific bHLH proteins. Plant Cell 19(2): 429–441 (2007).

12. Okushima, Y.; Fukaki, H.; Onoda, M.; et al. ARF7 and ARF19 regulate lateral root formation via direct activation of LBD/ASL genes in Arabidopsis. Plant Cell 19(1): 118–130 (2007).

13. Thatcher, L. F.; Kazan, K.; Manners, J. M. LBD20 is involved in plant defense responses. Plant Physiol. 158(3): 1195–1205 (2012).

14. Hu, Y.; Zhang, J.; Jia, H.; et al. Lateral organ boundaries 1 is a disease susceptibility gene for citrus bacterial canker disease. Nat. Commun. 5: 3117 (2014).

15. Bera, S. K.; Kamdar, J. H.; Kasundra, S. V.; et al. Identification of groundnut genotypes and wild species resistant to stem rot using an efficient field screening technique. Electron. J. Plant Breed. 7(1): 61–70 (2016).

16. Gorbet, D. W.; Kucharek, T. A.; Shokes, F. M.; et al. Field evaluations of peanut germplasm for resistance to stem rot caused by Sclerotium rolfsii. Peanut Sci. 31(2): 91–95 (2004).

17. Ferrar, P. H.; Walker, J. R. L. o-Diphenol oxidase inhibition—an additional role for oxalic acid in the

phytopathogenic arsenal of Sclerotinia sclerotiorum and Sclerotium rolfsii. Physiol. Mol. Plant Pathol. 43(6): 415–422 (1993).

18. Bateman, D. F.; Beer, S. V. Simultaneous production and synergistic action of oxalic acid and polygalacturonase during pathogenesis by Sclerotium rolfsii. Phytopathology 55(11): 204–211 (1965).

19. Lee, H. W.; Kim, J. Expansin A17, up-regulated by LBD18/ASL20, promotes lateral root formation during the auxin response. Plant Cell Physiol. 54(10): 1600–1611 (2013).

20. Shuai, B.; Reynaga-Peña, C. G.; Springer, P. S. The lateral organ boundaries gene defines a novel, plant-specific gene family. Plant Physiol. 129(2): 747–760 (2002).

21. Semiarti, E.; Ueno, Y.; Tsukaya, H.; et al. The ASYMMETRIC LEAVES2 gene of Arabidopsis thaliana regulates formation of a symmetric lamina, establishment of venation and repression of meristem-related homeobox genes in leaves. Development 128(10): 1771–1783 (2001).

22. Iwakawa, H.; Ueno, Y.; Semiarti, E.; et al. The ASYMMETRIC LEAVES2 gene of Arabidopsis thaliana encodes a member of a novel family of proteins characterized by cysteine repeats and a leucine zipper. Plant Cell Physiol. 43(5): 467–478 (2002).

23. Fan, M.; Xu, C.; Xu, K.; et al. Lateral organ boundaries domain transcription factors direct callus formation in Arabidopsis regeneration. Cell Res. 22(7): 1169–1180 (2012).

24. Xu, C. Y.; Cao, H. F.; Zhang, Q. Q.; et al. Control of auxin-induced callus formation by the bZIP59–LBD complex in Arabidopsis regeneration. Nat. Plants 4(2): 108–115 (2018).

25. Lee, H. W.; Kim, M. J.; Kim, N. Y.; et al. LBD18 acts as a transcriptional activator that directly binds to the EXPANSIN14 promoter to promote lateral root emergence in Arabidopsis. Plant J. 73(2): 212–224 (2013).

26. Chen, C.; Wu, Y.; Li, J.; et al. TBtools-II: A ‘one for all, all for one’ bioinformatics platform for biological big-data mining. Mol. Plant 16(11): 1733–1742 (2023).

27. Lescot, M.; Déhais, P.; Thijs, G.; et al. PlantCARE: A database of plant cis-acting regulatory elements and a portal to tools for in silico analysis of promoter sequences. Nucleic Acids Res. 30(1): 325–327 (2002).

28. Qi, X.-Y.; Chen, S.-S.; Feng, J.; et al. Selection and validation of reference genes for RT-qPCR in jasmine. Acta Agric. Boreali-Sin. 35(6): 22–30 (2020). [in Chinese]

29. Chen, S.; Zhou, Y.; Chen, Y.; Gu, J. fastp: an ultra-fast all-in-one FASTQ preprocessor. Bioinformatics 34(17): i884–i890 (2018).

30. Kim, D.; Langmead, B.; Salzberg, S. L. HISAT: a fast spliced aligner with low memory requirements. Nat. Methods 12(4): 357–360 (2015).

31. Liao, Y.; Smyth, G. K.; Shi, W. featureCounts: an efficient general-purpose program for assigning sequence reads to genomic features. Bioinformatics 30(7): 923–930 (2014).

32. Love, M. I.; Huber, W.; Anders, S. Moderated estimation of fold change and dispersion for RNA-seq data with DESeq2. Genome Biol. 15(12): 550 (2014).

33. Kanehisa, M. & Goto, S. KEGG: Kyoto Encyclopedia of Genes and Genomes. Nucleic Acids Res. 28, 27–30 (2000).

34. Kanehisa, M., Furumichi, M., Sato, Y., Kawashima, M. & Ishiguro-Watanabe, M. KEGG for taxonomy-based analysis of pathways and genomes. Nucleic Acids Res. 52, D366–D372 (2024).

35. Kanehisa, M.; Araki, M.; Goto, S.; et al. KEGG for linking genomes to life and the environment. Nucleic Acids Res. 36(Database issue): D480–D484 (2008).

36. Ashburner, M.; Ball, C. A.; Blake, J. A.; et al. Gene Ontology: tool for the unification of biology. Nat. Genet. 25(1): 25–29 (2000).

37. Li, Y.; Zhou, C.; Yan, X.; et al. Simultaneous analysis of ten phytohormones in Sargassum horneri by HPLC-ESI-MS/MS. J. Sep. Sci. 39(10): 1804–1813 (2016).

38. Cai, B.-D.; Zhu, J.-X.; Gao, Q.; et al. Rapid determination of cytokinins in Oryza sativa by magnetic solid-phase extraction. J. Chromatogr. A 1340: 146–150 (2014).
39. Pan, X. Q.; Welti, R.; Wang, X. Quantitative analysis of major plant hormones in crude plant extracts by HPLC–MS. Nat. Protoc. 5(6): 986–992 (2010).
40. Niu, Q.; Zong, Y.; Qian, M.; Yang, F.; Teng, Y. Simultaneous quantitative determination of major plant hormones in pear flowers and fruit by UPLC/ESI-MS/MS. Anal. Methods 6(6): 1766–1773 (2014).
41. Šimura, J.; Antoniadi, I.; Široká, J.; et al. Plant hormonomics: multiple phytohormone profiling by targeted metabolomics. Plant Physiol. 177(2): 476–489 (2018).
42. Floková, K.; Tarkowská, D.; Miersch, O.; et al. Target profiling of stress-induced phytohormones by UHPLC-MS/MS. Phytochemistry 105: 147–157 (2014).
43. Cui, K.; Lin, Y.; Zhang, X.; et al. Comparison of pretreatment methods for phytohormones in plants by LC-ESI-MS/MS. Microchem. J. 121: 25–31 (2015).
44. Xiao, H.-M.; Cai, W.-J.; Ye, T.-T.; Ding, J.; Feng, Y.-Q. Spatio-temporal profiling of ABA, IAA and JA in a single rice seed during germination by UPLC-MS/MS. Anal. Chim. Acta 1031: 119–127 (2018).
45. González, I.; Déjean, S.; Martin, P.; Baccini, A. CCA: an R package to extend canonical correlation analysis. J. Stat. Softw. 23(12): 1–14 (2008).
46. Jozefczuk, S.; Klie, S.; Catchpole, G.; et al. Metabolomic and transcriptomic stress response of Escherichia coli. Mol. Syst. Biol. 6: 364 (2010).
47. Bouhaddani, S.; Houwing-Duistermaat, J.; Salo, P.; Perola, M.; Jongbloed, G.; Uh, H. W. Evaluation of O2PLS in omics data integration. BMC Bioinformatics 17(Suppl 2): S11 (2016).
48. Rabinowitz, J. S.; Robitaille, A. M.; Wang, Y.; et al. Transcriptomic, proteomic, and metabolomic landscape of positional memory in the caudal fin of zebrafish. Proc. Natl Acad. Sci. USA 114(5): E717–E726 (2017).

Author contributions statement

J. H. designed the study, performed most experiments, analyzed the data, and wrote the manuscript. Q.S. contributed to the experimental design and participated in the experiments. M.S. provided the Sclerotium rolfsii strain. Y.Z. and Y.H.Z. participated in the inoculation experiment. C.L. contributed to the experimental design, participated in the inoculation experiment, and supervised the research. Z.J. and Z.B. discussed and defined the overall research direction and supervised the research; Z.B. acquired funding. All authors reviewed and approved the final manuscript.

Funding

This work was supported by the Guangxi Science and Technology Department, Guangxi Zhuang Autonomous Region Government, through the Guangxi Science and Technology Program “Establishment of the Jasmine Research Institute” (Grant No. Guike AD19245202) and “Innovation and Application of Jasmine Quality Improvement and Efficiency Enhancement Technologies” (Grant No. Guike AB18221064).

Competing interests

The authors declare no competing interests.

Data availability

The Illumina RNA-sequencing raw data of *Jasminum sambac* (double-petal cultivar) at three infection stages (0 h, 48 h, and 96 h, each with three biological replicates) have been deposited in the **NCBI Sequence Read Archive**

(SRA) under the **BioProject accession PRJNA1337283** (http://www.ncbi.nlm.nih.gov/bioproject/1337283), with associated **BioSample accessions** SAMN52350555, SAMN52350556, SAMN52350557, SAMN52350558, SAMN52350559, SAMN52350560, SAMN52350561, SAMN52350562, and SAMN52350563.

Additional information

Correspondence and requests for materials should be addressed to *[J.H.] ([*649252488@qq.com*])*.

Supplementary Files

This is a list of supplementary files associated with this preprint. Click to download.

- FigureS1A.ChromosomaldistributionofLBDfamilygenesinjasmineHtLBD.png
- FigureS1B.ChromosomaldistributionofLBDfamilygenesinjasmineSJLBD.png
- FigureS1C.ChromosomaldistributionofLBDfamilygenesinjasmineDJLBD.png
- FigureS2A.DistributionofcisactingelementsinpromotersofjasmineLBDfamilygenesHTLBD.png
- FigureS2B.DistributionofcisactingelementsinpromotersofjasmineLBDfamilygenesSjLBD.png
- FigureS2C.DistributionofcisactingelementsinpromotersofjasmineLBDfamilygenesDjLBD.png
- FigureS3A.PredictedtranscriptionfactorbindingsitesTFBSsinpromotersofjasmineLBDfamilygenesHtLBD.png
- FigureS3B.PredictedtranscriptionfactorbindingsitesTFBSsinpromotersofjasmineLBDfamilygenesSjLBD.png
- FigureS3C.PredictedtranscriptionfactorbindingsitesTFBSsinpromotersofjasmineLBDfamilygenesDjLBD.png
- FigureS4ASyntenycollinearityanalysisofLBDgenesHt.png
- FigureS4BSyntenycollinearityanalysisofLBDgenesSj.png
- FigureS4CSyntenycollinearityanalysisofLBDgenesDj.png
- FigureS4DSyntenycollinearityanalysisofLBDgenesHtOryAth.png
- FigureS4ESyntenycollinearityanalysisofLBDgenesSjOryAth.png
- FigureS4FSyntenycollinearityanalysisofLBDgenesDjOryAth.png
- FigureS5AVolcanoplotofdifferentialmetabolitesinjasmineyoungstems0hvs48h.png
- FigureS5BVolcanoplotofdifferentialmetabolitesinjasmineyoungstems0hvs96h.png
- FigureS5CVolcanoplotofdifferentialmetabolitesinjasmineyoungstems48hvs96h.png
- FigureS6AGOenrichmentbubbleplotofDEGs0hvs48h.png
- FigureS6BGOenrichmentbubbleplotofDEGs0hvs96h..png
- FigureS6CGOenrichmentbubbleplotofDEGs48hvs96h.png
- FigureS7AKEGGenrichmentbubbleplotofDEGs0hvs48h.png
- FigureS7BKEGGenrichmentbubbleplotofDEGs0hvs96h.png
- FigureS7CKEGGenrichmentbubbleplotofDEGs48hvs96h.png
- tableS1PhysicochemicalpropertiesandpredictedsubcellularlocalizationofLBDfamilyproteinsinjasmine.xlsx
- TableS2KaKsratiosofsyntenicLBDgenepairsinHutousinglepetalanddoublepetaljasmine..xlsx
- GenomeHutou.zip
- GenomeSinglepetal.zip
- GenomeDoublepetal.zip
- SupplementaryData1DifferentialGenes48hvs0h.xlsx
- SupplementaryData2DifferentialGenes96hvs0h.xlsx
- SupplementaryData3DifferentialGenes96hvs48h.xlsx
- SupplementaryData4AllGenesFPKMexpressionmatrix.xlsx

- SupplementaryData5DifferentialMetabolites48hvs0h.xlsx
- SupplementaryData6DifferentialMetabolites96hvs0h.xlsx
- SupplementaryData7DifferentialMetabolites96hvs48h.xlsx
- SupplementaryData8TargetedMetabolitesContentMatrix.xlsx
- README.txt